

Self-consistent relativistic APW calculation of the electronic structure of niobium with a non-muffin-tin potential* †

N. Elyashar[‡]

University of Illinois, Chicago Circle, Chicago, Illinois 60680
and Argonne National Laboratory, Argonne, Illinois 60439

D. D. Koelling

Argonne National Laboratory, Argonne, Illinois 60439

(Received 24 November 1976)

We report the results of a self-consistent relativistic augmented-plane-wave calculation of the electronic structure of Nb. This calculation was performed using potentials and charge densities of general shape; i.e., the muffin-tin approximations of a spherical shape inside the muffin-tin spheres and constant in the interstitial region were *both* removed. The results are thus an accurate representation of the Hohenberg-Kohn-Sham formalism for Nb. We find that the results are generally better than those obtained using the full Slater ($\alpha = 1$) overlapping-charge-density model. The effects of small changes in exchange parameter α and lattice constant a have also been calculated.

I. INTRODUCTION

As the element with the highest known superconducting transition temperature, the electronic structure of Nb deserves careful attention. It has thus far been studied by magnetothermal¹ and de Haas-van Alphen¹⁻⁴ experiments; magnetoresistance,^{5,6} Kohn anomaly,⁷ photoemission,⁸ positron annihilation,⁹ Compton profile,¹⁰ optical reflectivity,¹¹ x-ray,¹²⁻¹⁵ plasmon,¹⁶ Knight shift,¹⁷ and resistivity studies.¹⁸ The interpretation of these amassed data has been facilitated by the numerous band calculations which have been performed.¹⁹⁻²⁸ The pioneering work of Mattheiss¹⁹ based on the overlapping-charge-density model with full Slater exchange²⁹ has served as the primary basis for all analysis as it was performed quite early and has proven very accurate. It has, in fact, been shown to be very close to the results of a self-consistent calculation²³ using the reduced Kohn-Sham-Gaspär^{30,31} (KSG) exchange. Mattheiss's results have also been fit by linear-combination-of-atomic-orbitals interpolation scheme and do quite well in interpreting the optical data.²⁵ They were also used as a basis for an attempt³² to understand the unusual phonon structure (dip) in Nb. (This interpretation is subject to question, however.²⁴) The potential of Deegan and Twose²⁰ was created using the same model as Mattheiss except at a slightly larger lattice constant. Their use of it was merely to test their modified orthogonalized-plane-wave method. It was used for a similar purpose by Euwema for his plane-wave-Gaussian method.²¹ The only physical application of this potential was by Cooke *et al.*,²² using a combined Korringa-Kohn-Rostoker linear-combination-of-

atomic-orbitals scheme to calculate the dielectric response. Anderson *et al.*,²³ and Wakoh *et al.*²⁶ have performed self-consistent calculations. Anderson *et al.*²³ performed their calculations for both full Slater and KSG exchange and for normal and reduced lattice constant. Their results agreed reasonably well with the experimental Fermi-surface data. Using this potential, the dielectric response function has been calculated²⁴ with equal or better success than that from the Mattheiss potential.²² Wakoh *et al.*²⁶ performed a self-consistent-field (SCF) calculation for $\alpha = 0.8$ ($\alpha = \frac{2}{3}$ for KSG and $\alpha = 1$ for full Slater exchange) but then introduced shifts of 0.02 Ry for the $d\epsilon$ (t_{2g}) and 0.04 Ry for the $d\gamma$ (ϵ_g) resonances as was done³³ for V and Cr in order to get good Fermi-surface areas. The fact that they obtained good agreement with positron annihilation⁹ and Compton¹⁰ anisotropy indicates that this has been successful.

The calculations of Painter *et al.*²⁷ and of Elyashar and Koelling²⁸ (hereafter referred to as I) were both performed using the full Slater-exchange overlapping-charge-density model to test the sensitivity of the band structure to non-muffin-tin effects. In I, we also included the relativistic effects and found that when both effects were included, the calculated results exhibited two additional de Haas-van Alphen orbits. These orbits were tentatively linked to the experimental data observed in the region near the [100] direction. This will be discussed in further detail below.

In this paper, we report the results of relativistic self-consistent calculations with no shape (i.e., muffin-tin) approximations. There are basically two reasons for performing these calculations. The first is the desire to have a calcula-

tion for the electronic structure of this important material which is as precise as possible. The second is that, given a very precise calculation for the model, one can begin to truly assess the quality of the model. We believe that our calculation is the most precise transition-metal band-structure calculation to date and thus can give the tightest bounds currently available. The only other system being given careful consideration as a test of Hohenberg-Kohn-Sham theory is copper³⁴ but there the question of relativistic and non-muffin-tin effects is as yet unanswered. We would also claim that the augmented-plane-wave (APW) calculations utilize greater variational freedom than the linear-combination-of-atomic-orbitals calculations.

This second reason requires some elaboration. In actuality, it is a simple case of the principle that one tests a theory by making predictions about an experiment. The complication is that, for band theory, the computations involved in making those predictions are sufficiently complex that it is necessary to make further approximations—which gives some doubt concerning the faithfulness of the resultant predictions as a representation of the theory. Thus, in this paper, we will explicitly state the model (theory) being examined, fully discuss the approximations used, and then make a comparison to the available experimental data.

One method of deriving a single-particle Hamiltonian for treating many-electron systems is based on the generalized Thomas-Fermi formalism of Hohenberg, Kohn, and Sham.^{30,35} It has been extended to include the spin effects by von Barth and Hedin.³⁶ We here will consider using only the exchange effects in the exchange-correlation functional consistent with the original formulation³⁰ foregoing the more involved expressions available.^{36,37} We will also ignore any relativistic corrections to this functional although they are known to exist³⁸ and assume no net spin density anywhere. We thus will be dealing with the theory in its simplest (and most approximate) form which is what is most commonly in use today.

There are several conditions on the theory that make it more appropriate for a metal than for an atom—where it was initially tested.³⁹ The theory requires a slowly varying density (not satisfied near the nucleus) and a high density (not satisfied at large distances in the atom). The violation of the first condition does not appear to have seriously impacted the theory³⁶ although one must be concerned about calculations specifically sampling the charge density near the nucleus. The condition of high density is fulfilled in the metal. That it is not fulfilled in the atom ($\rho \rightarrow 0$ as $r \rightarrow \infty$) is the reason

why the value of α found in the atomic $X\alpha$ calculation is a generally decreasing function of Z .^{40,41} As Z is increased, the high-density region expands and the assumption of the theory is more nearly satisfied. (Insulators and semiconductors also suffer from low-density regions which is one additional reason workers in these fields are trying to get away from this type of theory.) On the other hand, the calculations and comparisons are more easily performed for atomic systems.

The appropriate results of the theory to be examined are the ground-state total energy and charge density. In an atom, one can compare to actual Hartree-Fock calculations for these quantities as well as experimental data. There are no adequate Hartree-Fock calculations for such a comparison in metals leaving only the comparison to x-ray form factors, cohesive energies, bulk moduli, and lattice constants.⁴² X-ray form factors are lacking or of inadequate precision. Cohesive energies suffer from the complication that one must then again face the problem of the atomic calculation and its limitations.⁴² Bulk-moduli and lattice-constant determinations involve a great deal more computation and are single numbers. This has been done, however, for the lighter metals⁴² and it is found that the model, in its more complex form^{36,37} does quite well.

Thus it is easier to focus initially on the Fermi-surface properties.⁴³ This, however, requires an additional leap of faith. The energy Lagrange parameter $\epsilon_n(\vec{k})$ in the total energy variational conditions

$$\begin{aligned} (t + v + \alpha C \rho^{1/3}) \psi_n(\vec{k}) &= \epsilon_n(\vec{k}) \psi_n(\vec{k}), \\ t &= c \vec{\alpha} \cdot \vec{p} + \frac{1}{2} c^2 (\beta - 1), \\ v &= 2 \left(\int d\vec{r}' \frac{\rho(\vec{r}')}{|\vec{r} - \vec{r}'|} - \sum_n \frac{Z_n}{|\vec{r} - \vec{R}_n|} \right), \\ C &= -3(3/\pi)^{1/3}, \quad \alpha = \frac{2}{3} \end{aligned} \quad (1)$$

is merely to maintain the proper number of particles. There is no formal proof to connect them with the quasiparticle excitation energies in Landau Fermi-liquid theory. This connection can only be anticipated if one follows the alternate averaged Hartree-Fock derivation of Eq. (1). Such a connection is motivated by a great deal of past success⁴⁴ but can certainly be questioned.^{45,46} Again, we take the simpler (more approximate and historical) option. This is further motivated by the fact that the improved theories assume the solution of this simpler problem as a starting point.

The theory is a self-consistent-field theory. That is, the N ψ_m 's obtained from Eq. (1) must yield the charge density used to construct v and $\rho^{1/3}$. As will be described, this has been done to

high precision. A serious limitation of previous calculations has been the use of the muffin-tin shape approximation for the charge density and potential which can easily be as large as the many-body effects.⁴⁵ This shape approximation has not been made here. In Sec. II, we examine in some detail the techniques and approximations used in this calculation. In Sec. III, the results will be presented and compared with existing experimental data. The more discursive aspects will be collected in Sec. IV.

II. CALCULATIONAL TECHNIQUES

In I, we discussed the techniques we used to construct a non-muffin-tin potential in the required dual representation from the charge density in this same representation and the inclusion of the non-muffin-tin terms into the secular equation. Thus, we here discuss only the creation of the charge density from the solutions of the previous potential.

The electronic density is considered in two parts: (i) a contribution ρ_{valence} due to the valence electrons, and (ii) a contribution ρ_{core} from the (assumed) spherically symmetric densities of the filled atomiclike core shells

$$\rho = \rho_{\text{valence}} + \rho_{\text{core}}. \quad (2)$$

The core density is given by

$$\rho_{\text{core}}(\vec{r}) = \sum_{\vec{R}} \rho_{\text{core}}^0(\vec{r} - \vec{R}), \quad (3)$$

where ρ_{core}^0 is the contribution from a single site. These are calculated anew at each stage of the self-consistency process. \vec{R} are the vectors of the direct lattice. We make two very common approximations in the treatment of the cores. We ignore the nonspherical components of the potential in solving for the radial solutions and we assume that the cores are spherical about each site. These approximations must certainly be valid for the deep cores and are assumed so for the upper core states which are about 3.5 Ry below the Fermi energy. In any case, these approximations have even been used for most (if not all) calculations on the tetrahedrally bonded semiconductors—a far worse case than we are dealing with here. The valence density is given by

$$\rho_{\text{valence}} = \sum_{\vec{n}\vec{k}} f_{\vec{n}\vec{k}} w_{\vec{k}} P_1 (\psi_{\vec{n}\vec{k}}^\dagger \psi_{\vec{n}\vec{k}} + \psi_{\vec{n}\vec{k}}^{\prime\dagger} \psi_{\vec{n}\vec{k}}^{\prime}), \quad (4)$$

where $\psi_{\vec{n}\vec{k}}$ is an eigenvector of the band Hamiltonian for the state having a reduced wave vector \vec{k} and a band index n , and $\psi_{\vec{n}\vec{k}}^{\prime}$ is the spin-flipped state. P_1 is the Γ_1 projection operator and $w_{\vec{k}}$ is an appropriately chosen weighting factor. The \vec{k} summation is over the irreducible wedge of the

Brillouin zone since we are summing only the cubic symmetric parts. $f_{\vec{n}\vec{k}}$ is the Fermi factor at $T=0$,

$$f_{\vec{n}\vec{k}} = \begin{cases} 1 & \text{for } E_{\vec{n}\vec{k}} \leq E_F, \\ 0 & \text{for } E_{\vec{n}\vec{k}} > E_F, \end{cases} \quad (5)$$

where E_F is the Fermi energy.

This density is to be written in the required dual representation

$$\rho(\vec{r}) = \begin{cases} \sum \rho_\nu(r) K_\nu(\hat{r}), & r \leq R_{\text{MT}}, \\ \sum_i \rho(\vec{K}_i) e^{i\vec{K}_i \cdot \vec{r}}, & r \geq R_{\text{MT}}, \end{cases} \quad (6)$$

where R_{MT} is the muffin tin (MT) sphere radius, \vec{K}_i are the reciprocal-lattice space vectors, and $K_\nu(\hat{r})$ are the cubic harmonics. It should be noted here that the muffin-tin sphere merely decomposes into two regions where different expansions are used. There has been no limitation to a muffin-tin potential or density.

The wave function is written

$$\psi_{\vec{k},n,s} = \begin{cases} \sum_{\kappa\mu} a_{\kappa\mu}(\vec{k},n,s) \begin{pmatrix} g_{\kappa n} \chi_\kappa^\mu \\ i\sigma_r(1/c)f_{\kappa,n}\chi_\kappa^\mu \end{pmatrix}, & r \leq R_{\text{MT}}, \\ \sum_{j s'} b_{j s'}(\vec{k},n,s) e^{i(\vec{k}+\vec{K}_j) \cdot \vec{r}} \begin{pmatrix} \chi(s') \\ \sim 0 \end{pmatrix}, & r \geq R_{\text{MT}}, \end{cases} \quad (7)$$

where κ and μ are the standard central-field quantum numbers,⁴⁷ $g_{\kappa n}$ and $f_{\kappa n}$ are the radial functions for \vec{k} and E_n , χ_κ^μ is the central field angular function,⁴⁷ and $\chi(s)$ is a spinor quantized along the z axis. The expansion coefficients are related by

$$a_{\kappa\mu} = 4\pi \sum_{n s'} i^l b_{n s'} C(\kappa\mu s') j(|\vec{k}+\vec{K}_n| R_{\text{MT}}) \times Y_l^{\mu-s'} \left(\frac{\vec{k}+\vec{K}_n}{|\vec{k}+\vec{K}_n|} \right), \quad (8)$$

$$l = \begin{cases} \kappa, & \kappa > 0, \\ -(\kappa+1), & \kappa < 0, \end{cases}$$

where j is a spherical Bessel function and C is a $j' = \frac{1}{2}$ Clebsch-Gordan coefficient which is completely specified by the arguments given (although this is not the standard notation). Then

$$\rho(\vec{r}) = \sum_{n, \vec{k}, \kappa, \kappa'} f_{\vec{n}\vec{k}} A_{\kappa\kappa'} w_{\vec{k}} \left(g_{\kappa n} g_{\kappa' n} + \frac{1}{c^2} f_{\kappa n} f_{\kappa' n} \right), \quad (9)$$

where the $A_{\kappa\kappa'}$ are given⁴⁸ by straightforward but tedious (and error-prone) angular-momentum considerations. The projection operator P_1 no longer needs to be explicitly included as it is already accounted for in the cubic harmonic projection

TABLE I. Convergence of density components (in a.u.) at the muffin-tin surface with the maximum angular momentum used from the wave function. This test was performed without including the core states. The wave functions actually used were those resulting from the overlapping-charge-density $\alpha = 1$ potential used in I.

L_{\max}	σ_0	σ_4	σ_6
2	2.7087	-0.2541	0.0
4	2.8027	-0.2824	-0.1114
6	2.8103	-0.5107	0.0055
8	2.8111	-0.5377	0.1356
10	2.8112	-0.5403	0.1476
∞^a	2.8114	-0.5404	0.1481

^aObtained from the plane-wave-expanded expression for the interstitial region.

implied by $A_{\kappa\kappa'\nu}$.

The interstitial plane-wave expansion is given by

$$\rho(\vec{K}_i) = \frac{1}{n_i} \sum_{n\vec{k}_s} f_{n\vec{k}_s} w_{\vec{k}_s} \sum_{i', i''} b_{i' s}^*(n\vec{k}_s) b_{i'' s}(n\vec{k}_s) \times \Delta(\vec{K}_i, (\vec{K}_{i'} - \vec{K}_{i''})), \quad (10)$$

where n_i is the number of elements in the star of \vec{K}_i and $\Delta(\vec{K}_1, \vec{K}_2)$ is zero unless \vec{K}_1 and \vec{K}_2 are in the same star when it is one. In this way we have performed the Γ_1 projection on the contribution from each $\psi_{\vec{k}, n, s}$ and thus need only sum over the $\frac{1}{48}$ th of the Brillouin zone.

It is useful to note that the two expressions of Eq. (6) for the density must yield the same value at the muffin-tin-sphere surface. This not only provides a useful check for errors in the computer programs but also a very good test for the convergence of the various summations. The expressions of Eq. (6) involve two different truncations (ν and K_n) and thus can give information about the effects of these truncations which we have discussed in I. But in addition, by using a Rayleigh decomposition of the plane waves, we can examine the (κ, κ') convergence for each ρ_ν in Eq. (9). The series is found to converge quite rapidly for the spherical part ($\nu=0, \kappa=\kappa'$) of the density. Carrying the positive and negative parts of the κ sums out to the same $l_{\max}=4$ yielded a result for this term which had no significant error. Unfortunately, the nonspherical terms cannot be so quickly truncated. With the same $l_{\max}=4$, they differed in sign from the corresponding plane-wave generated component. This difference is easily understood. The spherical part represents only the gross feature of the density and is a sum of rapidly diminishing nonnegative numbers. The nonspherical terms represent finer structure and involve sizable

cancellations. The l_{\max} convergence was tested over the range from 4 to 12. For $l_{\max} \geq 10$, the two expressions matched within one-tenth of a percent as can be seen in Table I.

The \vec{k} summation of Eq. (4) is a finite sampling representation of an integral. Thus some care should be used in the choice of the \vec{k} points used and weights assigned. We have chosen to use the traditional cubic mesh with the weights $w_{\vec{k}} = 48/n_{\vec{k}}$ where $n_{\vec{k}}$ is the order of the group of the \vec{k} vector. This choice is not only convenient but is actually the sum that would result from using periodic boundary conditions with finite cells containing N unit cells where N is the number of points in the full Brillouin zone. Mattheiss *et al.*⁴⁹ have estimated for MT calculations on fcc crystals that one will get millirydberg precision using 256 points in the Brillouin zone (19 in the irreducible wedge). We have thus chosen to use 55 points in the irreducible wedge (1024 points in the entire zone) throughout our calculations. This mesh is finer by a factor of 2 in linear dimension. It was used because the non-muffin-tin contributions are more sensitive⁵⁰ to Brillouin-zone sampling than the muffin-tin contribution—which is, after all, only the gross average. Our sampling is thus appropriate to periodic boundary conditions of a cell containing 1024 unit cells. There are, of course, other choices. One could array one's points as the centers of a set of tetrahedra, for example. Or one could include in $f_{n\vec{k}} w_{\vec{k}}$ information about the actual volume of occupied space "near \vec{k} ." Such refinements while interesting as to their effect, would require considerable additional computation to explore and thus were beyond the current scope of our endeavors. They are mentioned only to point out one approximation of this calculation.

One further approximation was made in order to be able to include the 4s and 4p levels into the core states—which results in a considerable savings of effort. These orbitals are not fully contained within the muffin-tin spheres. Thus we merely linearly extended the muffin-tin ($\nu=0$) potential and overlapped the single site orbitals. This amounts to neglecting the effect of the very small 4s and 4p bandwidth on the wavefunctions. For the 4p states, this was tested by numerical calculations the results of which are shown in Figs. 1 and 2. As can be seen the spherical part of the electron density is unaffected. There are small but quite acceptable errors for the nonspherical contributions.

III. RESULTS

A. Self-consistency

Three self-consistent calculations were actually performed. The first used a lattice constant a

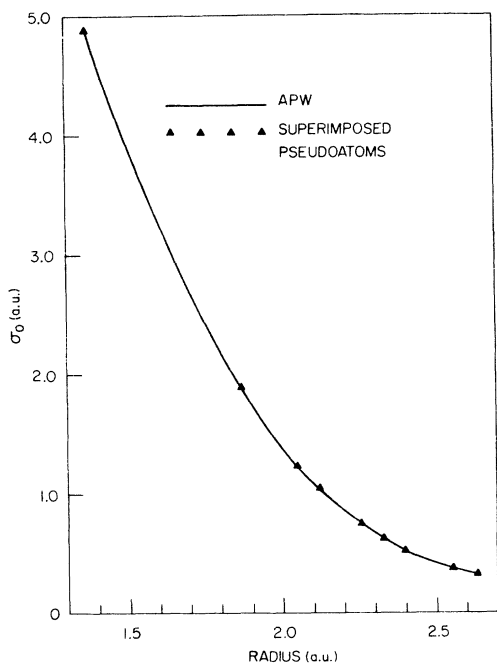


FIG. 1. Comparison of the spherical contribution to the density by the $4p$ states as calculated from the relativistic APW wave functions and from the single-site approximation described in the text. All densities within the MT sphere are plotted as $\sigma = 4\pi r^2 \rho$.

= 6.23774 a.u. with the KSG exchange ($\alpha = \frac{2}{3}$). This lattice constant was chosen the same as Anderson *et al.*²³ to facilitate comparison. To see the effect of a change in exchange scaling, a second calculation was performed using $\alpha = 0.705$ at this same lattice constant. A third calculation was performed using $\alpha = \frac{2}{3}$ but at a lattice constant of 6.2286 a.u. which we believe to be more appropriate to liquid-helium temperatures. These calculations will be identified as SCF(1), SCF(2), and SCF(3), respectively.

The first calculation was started using the overlapping charge density model constructed as described in I. The niobium atomic charge density was calculated assuming a d^4s^1 configuration with $\alpha = \frac{2}{3}$. The second and third calculations were started from the converged results of the first. The sensitivity of the calculation to the exchange scaling parameters α can be seen from the fact that it required six iterations to converge the $\alpha = 0.705$ calculation starting from the converged $\alpha = \frac{2}{3}$ charge density. The effect on the charge density was to pull an additional 0.025 electron into the muffin-tin sphere and *increase* the anisotropy by roughly 4%.

Because the SCF iterative process is normally unstable, it is necessary to provide some form of

damping. This was done by mixing the input and output densities of the n th iteration to form the input density to the $(n+1)$ th iteration

$$\rho_{n+1}^{\text{in}} = \beta \rho_n^{\text{out}} + (1 - \beta) \rho_n^{\text{in}}. \quad (11)$$

The mixing fraction β was varied from 0.25 at the beginning (where changes were large and much damping required) to 0.95 at the final iterations. Iterations were continued until no energy on our 55 point mesh changed by more than 0.0005 Ry and no component of the density changed by more than 0.1%. The second condition proved the more-stringent condition. In the first calculation, we continued to iterate beyond these conditions until the components were seen to oscillate about a mean. This was done to insure that there would not be small systematic shifts which could accumulate to a significant error. In all, we performed nine iterations on the first calculation but we had satisfied our criterion for convergence by the sixth iteration.

In the SCF process, we also observed the property²³ that the relaxation effects could be very well mimicked by increasing the exchange scaling α up from $\frac{2}{3}$. Its primary effect is to pull the upper d bands down relative to the s - p band (which is itself pulled down). There is, of course, a resultant narrowing of the d bands. An increase of α to 1 actually produces an effect greater than that produced by the relaxation. If one assumes that the effect is roughly linear in the overlapping-charge-density (OCD) model, then one should increase α by $\frac{2}{9}$ to mimic the SCF results. This

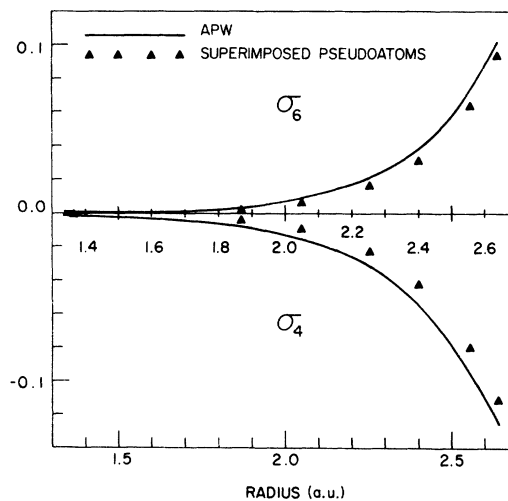


FIG. 2. Comparison of the nonspherical contribution to the density by the $4p$ states as calculated from the relativistic wave functions and from the single-site approximation described in the text. All densities within the MT sphere are plotted as $\sigma = 4\pi r^2 \rho$.

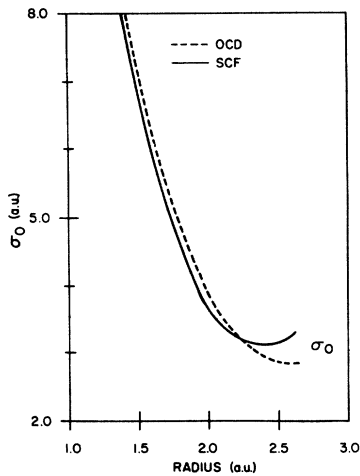


FIG. 3. Comparison of the spherical component of the density ($\sigma = 4\pi r^2 \rho$) within the MT sphere for the $\alpha = \frac{2}{3}$ overlapping-charge-density (OCD) model and the final SCF result.

mimicry is only valid for the energies, however. In going from the first iteration (or $\alpha = \frac{2}{3}$ OCD model) to the converged results, one finds that density is moved *out* of the MT sphere so that the charge in the interstitial region is increased from 1.249 electrons to 1.525 electrons. But increasing α in the OCD model moves charge *into* the MT sphere decreasing the interstitial density to 1.056 electrons for $\alpha = 1$. Thus, in order to adjust the energies, one increases the error in the wave functions.

In Figs. 3 and 4, the densities are presented

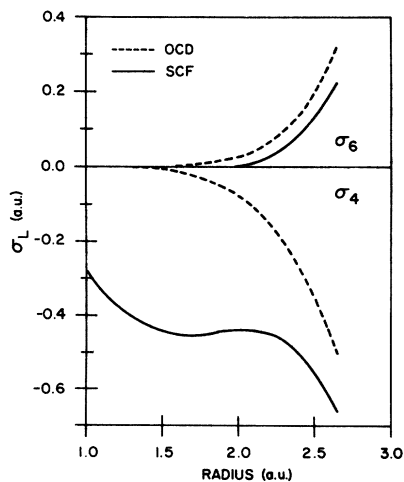


FIG. 4. Comparison of the nonspherical components of the density ($\sigma_L = 4\pi r^2 \rho_L$) within the MT sphere for the $\alpha = \frac{2}{3}$ overlapping-charge-density (OCD) model and the final SCF result.

both for the OCD model and the final SCF results. From the spherical component of Fig. 3, one also sees the net movement of density away from the nucleus consistent with the increase in the density in the interstitial region. The nonspherical components of Fig. 4 show another interesting feature. The $\nu = 6$ component shows a diminished asphericity in the SCF result as one might expect. The $\nu = 4$ component, however, is greatly increased. The major additional contribution in this case is from the fact that the Nb $4d$ states are not fully occupied and thus yield a sizable *intra*-atomic contribution to this nonspherical density. This is supported by the fact that the local maximum in the magnitude of σ_4 occurs at a radius of about 1.6 a.u. while the Nb $4d$ principal maximum occurs at about 1.55 a.u. This feature would normally not be included in any application of the OCD model as it is customary to overlap spherical charge densities. Its effect on the potential is shown in Fig. 5 where the nonspherical components are compared for the OCD model and the SCF calculation.

B. Comparison with other calculations

In Table II, we compare our results with those of other authors for selected energy separations. Because ours is the only relativistic calculation, it was necessary to remove the effects of spin-orbit coupling to make this comparison. Thus we have used $\Gamma_6^+ \rightarrow \Gamma_1$; $H_8^+ \rightarrow H_{12}$; $\frac{2}{3} \Gamma_8^+ + \frac{1}{3} \Gamma_7^+ \rightarrow \Gamma_{25'}$; and

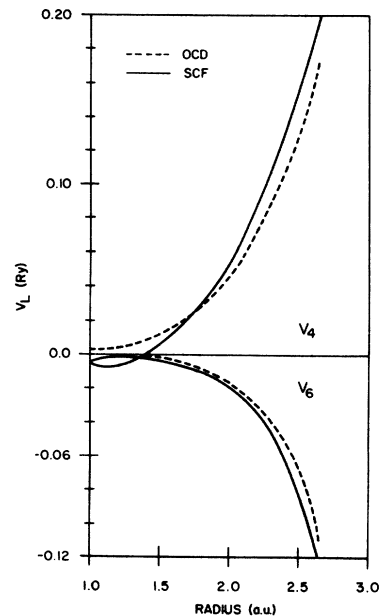


FIG. 5. Comparison of the nonspherical components of the potential for the $\alpha = \frac{2}{3}$ OCD model and the final SCF result.

TABLE II. Comparison of Nb band structures.

Ref.		a	α	$(\Gamma_{25'} - \Gamma_1)$	$(H_{25'} - \Gamma_1)$	$(H_{25'} - H_{12})$	$(E_F - H_{12})$	$(E_F - \Gamma_1)$
Present work	SCF(1)	6.237 74	$\frac{2}{3}$	471	865	700	277	442
	SCF(2)	6.237 74	0.705	463	850	688	274	436
	SCF(3)	6.2286	$\frac{2}{3}$	471	868	704	279	442
28	MT	6.237 74	1	457	810	660	271	421
28	GP ^a	6.237 74	1	443	806	648	259	417
19	MT	6.2294	1	420	770	660	280	390
20	MT		1	440	778	672		
23	MT	6.237 74	1	396	752	673	270	349
23	SCF	6.237 74	$\frac{2}{3}$	428	828	775	314	387
27	MT		1	388	736	645		
27	GP		1	380	735	634		
26	ADJ ^b		0.8	420	783	661	275	397
23/28	SCF ^c	6.237 74		444	854	763	302	413

^aGP, general potential.

^bThis calculation was an adjusted Green's function calculation. The adjustment consisted of shifting the t_{2g} phase shifts up by 0.02 Ry and the ϵ_g by 0.04 Ry.

^cSee text for an explanation of this entry.

$\frac{2}{3}H_8^+ + \frac{1}{3}H_7^+ \rightarrow H_{25'}$, as the necessary correspondences (see Fig. 6). The most interesting comparison is, of course, to the nonrelativistic muffin-tin self-consistent calculations of Anderson *et al.*²³ for $\alpha = \frac{2}{3}$. It was to facilitate this comparison that we chose to use the same (room-temperature) lattice constant for our first calculation. As can be seen, the results differ by a considerable amount. From the comparisons in I, one finds that the non-muffin-tin terms give rise to energy shifts which can be as large as 10–15 mRy. Most likely the non-muffin-tin effects are somewhat larger in the SCF calculation but it is difficult to believe that they could be much larger than about 20 mRy. This would seem to leave a sizable difference to the relativistic effects: too large, in fact, to believe. The resolution, we believe, lies in the fact that Anderson *et al.*²³ truncated the expansion used to start their radial integration at two terms. Too rapid a truncation of this series can cause s states to rise relative to the d states.⁵¹ Because the mesh used in the relativistic calculations extends to much smaller radii, this problem never occurs for us. By recalculating Γ_1 with the Anderson *et al.*²³ potential, we find a shift of 30 mRy. Thus, we have created an extra entry in Table I which includes this 30-mRy shift of Γ_1 and the general-potential-MT shifts of I as SCF. From this it would appear that the relativistic mass velocity and Darwin terms lower the s states by roughly 25 mRy and narrow the d bands by as much as 10%. This second effect is somewhat surprising since one might expect the relativistic effects to produce increased shielding of the nucleus for the d states causing them to extend more and thus be broader. But as such an argument depends on a very-tight-binding

picture with only first neighbor overlaps it very likely does not apply here. The agreement of the two calculations is, in general, quite good as can be seen from a simple consideration of the charge densities. We find that the muffin-tin component of the charge densities is not very different for the two SCF calculations. For example, the Anderson *et al.*²³ potential yields 1.50 electrons in the interstitial region where we obtained 1.525.

As there are no other relativistic band calculations for Nb, one can only compare the spin-orbit splitting to that of the atomic calculations. If the spin-orbit interaction is written

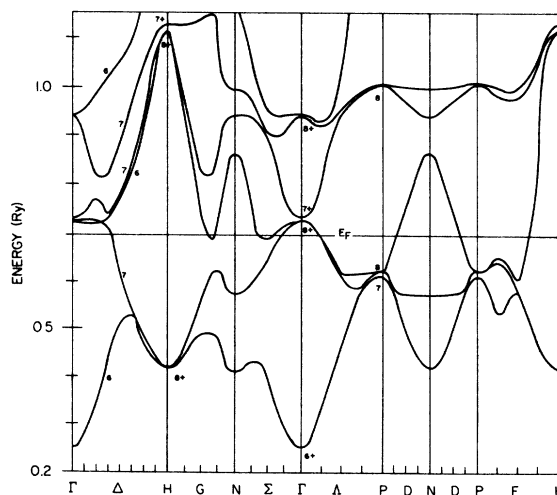


FIG. 6. SCF band structure resulting from the calculation performed using $\alpha = \frac{2}{3}$ with a lattice constant of 6.237 74 a.u.

$$H_{so} = \xi_L \vec{L} \cdot \vec{S}. \quad (12)$$

ξ_L then contains all the potential information. Then in the atom

$$\xi_d^{at} = \frac{2}{5} [E(d_{5/2}) - E(d_{3/2})] = 0.0044 \text{ Ry}, \quad (13)$$

and in the solid we split the triply degenerate $\Gamma_{25'}$, and should get

$$[E(\Gamma_7^*) - E(\Gamma_8^*)] = \frac{3}{2} \xi_d = 0.0066 \text{ Ry} \quad (14)$$

from tight-binding considerations.⁵² We find instead that this energy separation at Γ is 0.008 Ry—larger by just enough to perhaps be significant. This could be due either to the non-muffin-tin terms or to the deeper penetration of the d states into the core. The non-muffin-tin terms will provide an interaction between the $\Gamma_8^*(\Gamma_{12}) - \Gamma_8^*(\Gamma_{25'})$ states but not between the $\Gamma_8^*(\Gamma_{12}) - \Gamma_7^*(\Gamma_{25'})$ states thus increasing the splitting. On the other hand, an increased penetration into the muffin-tin sphere would also increase ξ_d because of the stronger potential experienced. This certainly occurs as one moves up in the band as can be seen from Andersen's treatment⁵³ of the spin-orbit parameter in band calculations or just from the fact that at the higher energy $H_{25'}$, $\xi_d = 0.008 \text{ Ry} \sim 2\xi_d^{at}$. This would also be consistent with the diminished value of σ_0 at small radii as seen in Fig. 3. Our $3d$ (core) splitting of 2.9 eV is within experimental error of the 2.8 eV observed by x-ray photoelectron spectroscopy.⁵⁴ We thus conclude that the treatment of the spin-orbit interaction is

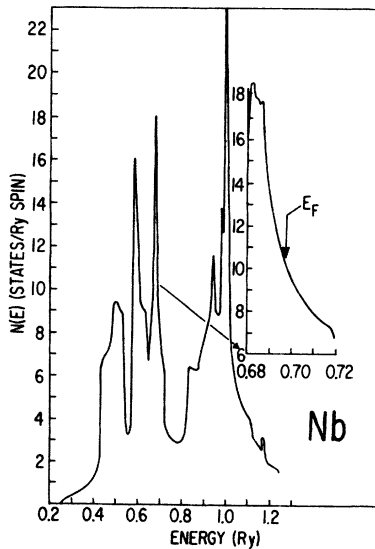


FIG. 7. Density of states for SCF(3) ($a = 6.2286$ and $\alpha = \frac{2}{3}$) calculated using the tetrahedron microzone technique applied to the Fourier-series representation of the bands. Inset gives greater detail about the Fermi energy (0.6975 Ry).

quite adequate.

To obtain a density of states, and hence the Fermi energy, we have fitted a Fourier series to the calculated data points and used that in a tetrahedron microzone scheme⁵⁵ [SCF(3)] or irrational vectors sampling [SCF(1) and SCF(2)]. For SCF(3), for example, we fitted 53 star functions (because of Γ_1 symmetry, the expansion coefficients of all members of a star are equal so that they may be combined into a single function for the star) to 120 points. These points were made up of the regular 55-point mesh plus a set scattered about the Fermi surface. The rms errors of the first six bands were 1–4 mRy with band 2 having 1.7-mRy and band 3, 2.1-mRy rms errors. The resultant density of states for SCF(3) is shown in Fig. 7. It yields a Fermi energy of 0.6975 Ry and a density of states of 10.2 states/Ry spin. Thus our SCF(3) results fall somewhat below the OCD ($\alpha = 1$) model results and more closely in line with the values found by other workers. This leaves a discrepancy from the McMillan value of 12.4. (It is of interest to note, however, that there are two discontinuities⁵⁶ in γ for Nb below 11 °K.)

We have also performed an approximate l decomposition for SCF(3) based on a j decomposition of the wave function within the muffin-tin spheres which was continued to the Wigner-Seitz sphere radius by continuation with the appropriate $V = 0$ solutions. They were combined for $j = l + \frac{1}{2}$ and $j = l - \frac{1}{2}$ to give a "fractional l character." When used as a weighting on the density-of-states calculation, one obtains the partial density of states often shown. This is, of course, only a very approximate description of wave-function character (not just computationally but conceptually) but it has proven useful. We thus found there to be 0.64 s , 0.68 p , 3.63 d , 0.12 f , and 0.03 g electrons in the conduction band. These numbers add to 5.07 electrons as a result of the very approximate nature of the calculations. This is in reasonable agreement with the results obtained by Nikiforov *et al.*,⁵⁷ using the Green's-function method with a potential similar, if not identical, to that of Mattheiss¹⁹: $n_s = 0.51$; $n_p = 0.61$; $n_d = 3.88$ if one scales their results for the interior of the muffin-tin sphere to the Wigner-Seitz sphere. (They get no f or g contribution as they truncate their basis set at $l = 2$.) Within the calculational errors, our results were essentially identical⁵⁸ to those obtained using the potential of Anderson *et al.*²³ Referring to the total density of states shown in Fig. 7, one sees the typical three-peak structure below the Fermi energy: the first (lowest in energy) is an s - d admixture with very slight p contribution on the high-energy side; the second is almost a pure d - p mixture; and the third is a d - p mixture.

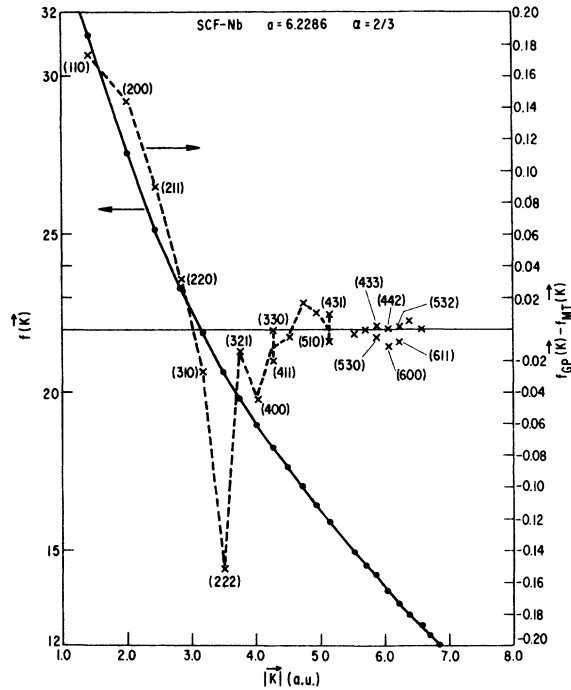


FIG. 8. X-ray form factors for Nb and the difference from a muffin-tin approximation.

ture with some f contribution but virtually no s at all.

In Fig. 8, we show the calculated x-ray form factors for the charge density resulting from SCF(3). The changes implied by the muffin-tin approximation to that density are also shown. Unfortunately, there is no experimental data available for comparison to the best of our knowledge. However, it is possible to argue by comparison to the vanadium results that the anisotropy might be too small by an order of magnitude.⁵⁹

C. Comparison to experiment

The only experimental data to which we will be comparing our results in any detail is the magnetothermal oscillation and de Haas-van Alphen data. In Table III, we compare the results obtained by direct relativistic APW orbit tracing for SCF(3) to the experimental results. Two remarks about Table III are in order. First, although the eigenvalues used in the tracing were for the actual general (shape) potential, the Hellman-Feynman calculations of the derivatives omitted the derivatives of the non-muffin-tin terms because of their complexity. This should yield only minor errors in the calculated masses—which will be largest for the octahedron. Second, the new octahedron and JG(N) results⁴ are preliminary results which are included for completeness. Further analysis is

being performed on the experimental data (and interpretation) so that they may have to be revised although we doubt it. As can be seen, the calculated ellipses are too large and the octahedron too small. This is the effect seen in I for the addition of the non-muffin-tin effects. The self-consistency has improved the situation somewhat, however, by moving some volume from the ellipses back to the octahedron. The jungle gym is seen to be generally too small. The values for dA/da must be considered very approximate as two different techniques were used to assign the Fermi energy for SCF(1) and SCF(3). Although the difference should be small (i.e., less than a mRy), it would still affect the results. Nonetheless, one can see that the effect is not uniform as would be obtained by a simple Fermi surface shift.

To make an easier comparison, we have tabulated in Table IV two error functionals:

$$\bar{\epsilon} = \left[\sum_i \left(\frac{1}{m_i^*} \right) |A_{\text{expt}}^i - A_{\text{calc}}^i| \right] / N\bar{A},$$

$$\sigma^2 = \left[\sum_i \left(\frac{1}{m_i^*} \right) (A_{\text{expt}}^i - A_{\text{calc}}^i)^2 \right] / N(\bar{A})^2, \quad (15)$$

$$N = \sum_i \left(\frac{1}{m_i^*} \right), \quad \bar{A} = \left(\sum_i \frac{1}{m_i^*} A_{\text{expt}}^i \right) / N,$$

which are weighted by the calculated band mass (to convert to an energy error as $\pi m^* = dA/dE$). The sum is over the areas given in Table III. Interestingly enough, the two OCD model calculations with the muffin-tin approximation give the best agreement with experiment. The SCF calculations with reduced exchange ($\alpha = \frac{2}{3}$) all are in roughly the same range. This would lead one to believe that an increase in exchange parameter should improve the calculated results—which one sees is not what happens [from SCF(2)]. This was especially puzzling to us in light of one (erroneous) calculation we performed. In one of our final iterations, an input card was incorrectly done which resulted in the d -orbital logarithmic derivatives being lowered by 3–5 mRy (and slightly narrowed). This “adjusted” calculation was the best of all, yielding an rms error of 3.2%! In a muffin-tin calculation, this should be the effect of increasing the exchange constant α . One possible resolution of this apparent discrepancy is that the non-muffin-tin effects have also been significantly increased. Thus the “good” effect of lowering the d bands is undone by the increase in the $\Gamma_{8+} - \Gamma_{8-}$ separation (which is a natural consequence of the non-muffin-tin effects). This very well may not be the whole story, however, as the same effect apparently appears in the muffin-tin SCF calculations.⁵⁹ It would thus appear that the SCF calculations are

TABLE III. Comparison of experimental and calculated de Haas–van Alphen areas (in a.u.) and masses (in electron masses). Areas were calculated using actual relativistic APW calculated points and derivatives.

Field direction	Label ^a	Expt.	Area		Mass	
			Calc.	dA/da	Expt.	Calc.
[100]	OCT(Γ) ^b	0.2793	0.2547	-0.34		-2.06
	ELL(N)	0.1787	0.1898	-0.35		-0.90
	ELL(N)	0.2277	0.2475	-0.004	-1.97	-0.96
	JG(Δ)	0.0389	0.0330	-0.07	-1.6	-0.56
	JG(N) ^c	0.4053	0.4201	0.14		1.77
[111]	OCT(Γ)	0.1352	0.1155	-0.23		-1.40
	ELL(N)	0.1803	0.1939	-0.33	-1.56	-0.71
	ELL(N)	0.2271	0.2446	-0.47		-1.08
	JG(Γ)	0.2317	0.2103	-0.42		-2.22
	JG(H)	0.5192	0.5110	-0.34		-1.12
[110]	OCT(Γ) ^b	0.2086	0.1884	-0.27		-1.66
	ELL(N)	0.1859	0.1978	-0.33	-1.4	-0.72
	ELL(N)	0.2131	0.2307	-0.37	-1.54	-0.80
	ELL(N)	0.2408	0.2574	-0.45		-0.93

^aNotation of Refs. 19 and 23. (The OCT refers to the so-called octchedral surface at Γ ; the ELL to the ellipses centered at N ; and the JG to the “jungle gym.”)

^bPreliminary results, Ref. 4.

^cThe experimental data is probably for a break-down orbit. The more probable value is 0.405 (Ref. 4).

producing d bands which have too large a band width which is only exacerbated by increasing the exchange parameter.

Finally, we should like to reexamine two interesting aspects of the experimental data in light of these calculations: the discontinuity in the η -orbit data and the small [100] frequencies (α , α' , and β). As discussed in I, the discontinuities in the η orbit data [JG(H)] can be related to a protrusion on the jungle gym arms. In Fig. 9, we show the η -orbit areas and masses obtained from the Fourier series fit to the bands. Although the protrusion is not well fit by the Fourier series (most of the error for band three came from this region), it is still possible to see the (qualitative) effect. Only the cusplike structure at 25 deg from the [101] direction shows up clearly although a very careful examination of the curves shows additional breaks at about 50 deg and between 60 and 65 deg. There is probably something occurring between 10 and 15 deg as well. The masses show clearly the discontinuity at 26 and 51 deg with some indication of the others. Because the orbit code automatically positions the origin of the orbit for an extremum we also can consider the question of whether the discontinuities are associated with a shift of the origin. There was observed a very slight shift in the region between 51 and ~65 deg and nowhere else. This lends some credence to the existence of a small discontinuity at that point which would probably be

more pronounced were the Fourier series to better resolve the structure in that region.

The [100] orbits are quite a puzzle. Most likely the β orbit is a breakdown and/or magnetic interaction frequency and the α orbit is to be associated with the minimum in the jungle gym arm. Accordingly, the β orbit has a very limited angular range about [100] whereas the α orbit can be seen a very long way out.⁴ Our calculated frequency (0.0330 a.u.) is consistent with the calculated jungle gym being somewhat too small. The α' frequency can perhaps be explained by the shallow minimum-

TABLE IV. Comparison of errors in de Haas–van Alphen found for different calculations.

Calculation	Error (%)		
	Average	rms	
$\alpha = 1$	OCD-NR-MT (Ref. 19)	4.4	5.7
	OCD-Rel-MT (I)	3.2	4.2
	OCD-Rel-GP (I)	9.4	10.0
$\alpha = \frac{2}{3}$	SCF-NR-MT (Ref. 23) ^a	6.8	9.3
	SCF-Rel-GP [SCF(3)]	7.0	7.2
	SCF-Rel-GP [SCF(1)]	6.6	7.0
$\alpha = 0.705$	SCF-Rel-GP [SCF(2)] ^b	7.0	7.9

^aJG(N) orbit not available and so omitted.

^bAreas and masses actually calculated from a Fourier-series fit.

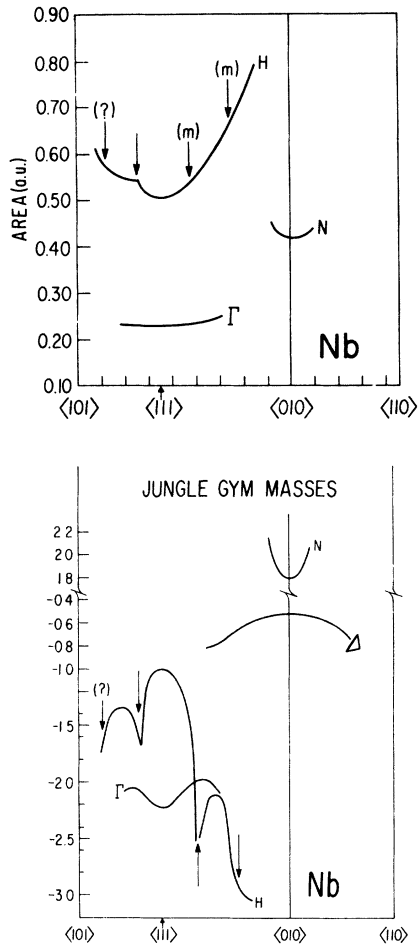


FIG. 9. de Haas-van Alphen frequencies and masses calculated for the jungle-gym surface. Calculations were performed using the Fourier-series fit to SCF(3). Points indicated by arrows are results of protrusion of surface roughly halfway from Γ to H as discussed in text. The points marked (m) indicate that the effect is best seen from the mass data.

maximum structure we observe on the octahedron. The minimum frequency (0.02509 a.u.) is so close to the maximum (0.02515 a.u.) that they would not be resolvable. These areas are too small consistent with the calculated octahedron being too small. The above areas were calculated by direct relativistic APW orbit tracing. From these calculations we find that the orbits (both JG and octahedron) are some what square shaped with the $[011]$ directions bulging out. The Fermi radius in

the $[001]$ direction is a monotonically decreasing function as one moves out the $[100]$ directions. The small increase in orbit area is thus due to the increase in the radius in the $[011]$ direction. Although these orbits are relatively minor features, they are occurring from a region of the Brillouin zone where bands are interacting and are thus very sensitive to inadequacies of the calculations. Thus they can be a very interesting feature as a test of any calculation.

IV. DISCUSSION

These calculations have demonstrated that well-known observation that a better calculation often does not lead to better agreement with experimental data. If one's main objective is the calculation of de Haas-van Alphen areas, a quick check of Table IV indicates that the overlapping charge density model with $\alpha = 1$ and a muffin-tin-shape approximation would give better results with far less effort. Proceeding to self-consistency reduces that agreement no matter whether you make the muffin-tin-shape approximation or not. Adjustments of the exchange scaling (α) do not appear to be able to help matters. Muffin-tin SCF calculations⁵⁹ on the group VB metals also indicate that the more involved $\alpha(\rho)$ -type calculations do not improve the agreement either. We ask about two major considerations concerning the situation: (i) Is this an observation of the fact that the de Haas-van Alphen effect reflects an excited state spectrum? or (ii) Is this the result of the limitations of a local density approximation? We believe it is the latter which is the significant feature. After all, a nonlocal interaction would smear out the effect of the density variations on the "potential" just like the muffin-tin-shape approximation does. Further, from our inadvertent computer experiment, it is seen that a very small l or j dependence in the potential could produce significant improvements in the results. This is the classic "nonlocal" effect in pseudopotential theory. Thus, we believe we are seeing, possibly for the first time, a concrete example of the limitations of a local density approximation.

ACKNOWLEDGMENTS

The authors are grateful to G. W. Crabtree, D. P. Karim, and J. B. Ketterson for the frequent and useful discussions throughout the course of this work. The access to their unpublished data is to be especially noted in addition.

- *Work supported by the U. S. Energy Research and Development Administration.
- †Paper based in part on a thesis submitted by one of the authors (N. Elyashar) in partial fulfillment of the requirements for the Ph.D. degree at the University of Illinois, Chicago Circle Campus.
- ‡Present address: Bailey Meter Co., Wickliffe, Ohio 44092.
- ¹M. M. Halloran, J. M. Condon, J. E. Graebner, J. E. Kunzler, and F. S. L. Hsu, *Phys. Rev. B* **1**, 369 (1970).
- ²G. B. Scott and M. Springford, *Proc. R. Soc. A* **320**, 115 (1970).
- ³J. R. Anderson and J. E. Schirber (unpublished).
- ⁴D. Karim, G. W. Crabtree, J. B. Ketterson, and L. R. Windmiller (unpublished).
- ⁵E. Fawcett, W. A. Reed, and R. R. Soden, *Phys. Rev.* **159**, 553 (1967); W. A. Reed and R. R. Soden, *ibid.* **173**, 677 (1968).
- ⁶N. E. Alekseevskii, K.-H. Bertel, and V. I. Nizhankovskii, *Zh. Eksp. Teor. Fiz. Pis'ma Red.* **19**, 117 (1974) [*JETP Lett.* **19**, 72 (1974)]; N. E. Alekseevskii, K.-H. Bertel, A. V. Dubrovin, and G. E. Karstens, *ibid.* **6**, 637 (1967) [*ibid.* **6**, 132 (1967)]; N. E. Alekseevskii, K.-H. Bertel, and A. V. Dubrovin, *ibid.* **10**, 116 (1969) [*ibid.* **10**, 74 (1969)].
- ⁷B. M. Powell, P. Martel, and A. D. B. Woods, *Phys. Rev.* **171**, 727 (1968).
- ⁸D. E. Eastman, *Solid State Commun.* **7**, 1697 (1969); I. Lindau and W. E. Spicer, *Phys. Rev. B* **10**, 2262 (1974).
- ⁹N. Shiotani, T. Okada, T. Mizoguchi, and H. Sekizawa, *J. Phys. Soc. Jpn.* **38**, 423 (1975).
- ¹⁰S. Wakoh, T. Fukamachi, S. Hosoya, and J. Yamashita, *J. Phys. Soc. Jpn.* **38**, 1601 (1975).
- ¹¹J. M. Weaver, D. W. Lynch, and C. G. Olsen, *Phys. Rev. B* **7**, 4311 (1973); **10**, 501 (1974).
- ¹²A. J. Golovashkin, J. E. Leksina, G. P. Motulevich, and A. A. Shubin, *Zh. Eksp. Teor. Fiz.* **56**, 51 (1969) [*Sov. Phys.-JETP* **29**, 27 (1969)]; F. J. Vilesov, A. A. Azgrubdkii, and M. M. Kirillova, *Opt. Spektrosk.* **23**, 153 (1967) [*Opt. Spectrosc.* **23**, 79 (1967)]; M. M. Kirillova and B. A. Charikov, *Fiz. Metal. Metalloved* **19**, 495 (1965) [*Phys. Met. Metallogr.* **19**, 13 (1965)].
- ¹³J. E. Holiday, *The Electron Microprobe*, edited by T. D. McKinley, K. F. J. Meinrich, and D. B. Wittry (Wiley, New York, 1966), p. 10; *Proceedings of the International Meeting on Electronic Structure of Metals and Alloys Studied by Methods of Band Structure Spectroscopy Methods at Strathclyde*, United Kingdom, edited by D. J. Fabian (Academic, New York, 1973), p. 251; J. E. Holliday, *Soft X-Ray Band Spectra and the Electronic Structure of Metals and Materials*, edited by D. J. Fabian (Academic, London, 1968), pp. 101-132.
- ¹⁴V. V. Nemoshkalkenko and V. P. Krivitskii, *Ukr. Fiz. Zh.* **13**, 1274 (1968) [*Ukr. Phys. J.* **13**, 911 (1968)]; V. V. Nemoshkalkenko, V. P. Krivitskii, A. P. Nesen-yuk, L. I. Nikolaev, and A. P. Shpak, *J. Phys. Chem. Solids* **36**, 277 (1975); A. P. Lukirskii and T. M. Zimkina, *Izv. Adad. Nauk SSSR* **27**, 330 (1963) [*Bull. Acad. Sci. USSR* **27**, 339 (1963)]; A. P. Lukirskii and J. A. Brytov, *Fiz. Tverd. Tela* **8**, 95 (1966) [*Sov. Phys.-Solid State* **8**, 72 (1966)]; V. A. Fomichev, A. V. Rudnev, and S. A. Nemnonov, *Izv. Akad. Nauk SSSR* **36**, 291 (1972) [*Bull. Acad. Sci. USSR* **36**, 268 (1974)]; M. J. Kursinskii and Y. E. Genkin, *ibid.* **25**, 1028 (1961) [*ibid.* **25**, 1033 (1961)]; A. V. Rudnev, V. A. Fomichev, and S. A. Nemnanov, *Fiz. Tverd. Tela* **13**, 2483 (1971) [*Sov. Phys.-Solid State* **13**, 2083 (1972)].
- ¹⁵R. Caillat, R. Fontaine, L. Feve, and M. J. Guittet, *C. R. Hebd. Seances Acad. Sci. C* **280**, 189 (1975).
- ¹⁶H. R. Apherholte and K. Ulmer, *Phys. Lett.* **22**, 552 (1966); M. J. Lynch and J. B. Swan, *Austr. J. Phys.* **21**, 811 (1968); V. V. Zashkvara, M. I. Korsunski, V. S. Red'kin, and V. E. Masyagin, *Fiz. Tverd. Tela* **11**, 3667 (1969) [*Sov. Phys.-Solid State* **11**, 3083 (1970)]; A. R. Shulman, V. V. Korablev, and Yu. A. Morozov, *Izv. Akad. Nauk SSSR* **35**, 218 (1971) [*Bull. Acad. Sci. USSR* **35**, 199 (1971)]; H. Claus and K. Ulmer, *Z. Phys.* **173**, 462 (1962).
- ¹⁷T. Kushida and J. C. Murphy, *Phys. Rev. B* **3**, 1574 (1971).
- ¹⁸W. R. Cox, D. J. Hayes, and F. R. Brotzen, *Phys. Rev. B* **7**, 3580 (1973); N. Morton, B. W. James, G. H. Wastenholm, and R. J. Nichols, *J. Phys. F* **5**, 85 (1975).
- ¹⁹L. F. Mattheiss, *Phys. Rev. B* **1**, 373 (1970); *AIP Conf. Proc.* **4**, 57 (1972).
- ²⁰R. A. Deegan and W. D. Twose, *Phys. Rev.* **164**, 993 (1967).
- ²¹R. N. Euwema, *Phys. Rev. B* **4**, 4332 (1971).
- ²²J. F. Cooke, H. L. Davis, and M. Mostoller, *Phys. Rev. B* **9**, 2485 (1974).
- ²³J. R. Anderson, D. A. Papaconstantopoulos, J. W. McCaffrey, and J. E. Schirber, *Phys. Rev. B* **7**, 5115 (1973).
- ²⁴S. K. Sinha and B. N. Harmon (unpublished).
- ²⁵W. E. Pickett and P. B. Allen, *Phys. Lett. A* **18**, 91 (1974); *Phys. Rev. B* **11**, 3599 (1975).
- ²⁶S. Wakoh, Y. Kubo, and J. Yamashita, *J. Phys. Soc. Jpn.* **38**, 416 (1975).
- ²⁷G. S. Painter, J. S. Faulkner, and G. M. Stocks, *Phys. Rev. B* **9**, 2448 (1974).
- ²⁸N. Elyashar and D. D. Koelling, *Phys. Rev. B* **13**, 5362 (1976).
- ²⁹J. C. Slater, *Phys. Rev.* **81**, 386 (1951).
- ³⁰W. Kohn and L. J. Sham, *Phys. Rev.* **140**, A1133 (1965).
- ³¹R. Gaspâr, *Acta Phys. Acad. Sci. Hung.* **3**, 263 (1954).
- ³²S. T. Chui, *Phys. Rev. B* **9**, 3303 (1975).
- ³³S. Wakoh and J. Yamashita, *J. Phys. Soc. Jpn.* **35**, 1394 (1973). (Nb is also briefly discussed.)
- ³⁴J. F. Janak, A. R. Williams, and V. L. Moruzzi, *Phys. Rev. B* **11**, 1522 (1975).
- ³⁵P. Hohenberg and W. Kohn, *Phys. Rev.* **136**, B864 (1964).
- ³⁶U. von Barth and L. Hedin, *J. Phys. C* **5**, 1629 (1972).
- ³⁷L. Hedin and S. Lundqvist, *J. Phys. C* **4**, 2064 (1971).
- ³⁸L. D. Miller, *Phys. Rev. A* **7**, 1433 (1973); D. E. Ellis, *J. Phys. B* (to be published).
- ³⁹B. Y. Tong and L. J. Sham, *Phys. Rev.* **144**, 1 (1966).
- ⁴⁰E. A. Kmetko, *Phys. Rev. A* **1**, 37 (1970).
- ⁴¹K. Schwartz, *Phys. Rev. B* **5**, 2466 (1972).
- ⁴²J. F. Janak, V. L. Moruzzi, and A. R. Williams, *Phys. Rev. B* **12**, 1257 (1975); V. L. Moruzzi, A. R. Williams, and J. F. Janak, *Bull. Am. Phys. Soc.* **21**, 307 (1976); *Phys. Rev. Lett.* (to be published).
- ⁴³J. F. Janak, A. R. Williams, and V. L. Moruzzi, *Phys.*

- Rev. B 6, 4367 (1972).
- ⁴⁴J. O. Dimmock, *Solid State Phys.* 26, 103 (1971).
- ⁴⁵G. Arbman and U. von Barth, *Nuovo Cimento* 23B, 37 (1974).
- ⁴⁶M. Rasolt and S. H. Vosko, *Phys. Rev. Lett.* 32, 297 (1974); *Phys. Rev. B* 10, 4195 (1974).
- ⁴⁷M. E. Rose, *Relativistic Electron Theory* (Wiley, New York, 1961).
- ⁴⁸N. Elyashar, Ph.D. thesis (University of Illinois, Chicago Circle Campus, 1975) (unpublished).
- ⁴⁹L. F. Mattheiss, A. C. Switendick, and J. H. Wood, *Methods in Computational Physics*, Vol. VIII, edited by B. Adler, S. Fernback, and M. Rotenberg, (Academic, New York, 1968).
- ⁵⁰B. N. Harmon, N. Elyashar, D. D. Koelling, *Bull. Am. Phys. Soc.* 20, 364 (1975).
- ⁵¹F. C. Griesen, *Phys. Status Solidi* 25, 753 (1968).
- ⁵²J. Friedel, P. Langhart, and G. Lehman, *J. Phys. Chem. Solids* 25, 781 (1964); L. F. Mattheiss and R. Watson, *Phys. Rev. Lett.* 13, 526 (1964); F. Herman and S. Skillman, *Atomic Structure Calculations* (Prentice-Hall, Englewood Cliffs, N. J., 1963).
- ⁵³O. K. Andersen, *Phys. Rev. B* 2, 883 (1970).
- ⁵⁴R. Caillat, R. Fontaine, L. Feve, M. J. Guillet, C. R. Acad. Sci. Paris 280, 189 (1975).
- ⁵⁵G. Lehmann and M. Taut, *Phys. Status Solidi* 54, 469 (1972); G. Lehmann, P. Rennert, M. Taut, and H. H. Wohn, *Phys. Status Solidi* 37, K27 (1970); O. Jepsen and O. K. Andersen, *Solid State Commun.* 9, 1763 (1971); J. Rath and A. J. Freeman, *Phys. Rev. B* 11, 2109 (1975).
- ⁵⁶H. A. Leupold, J. T. Breslin, G. J. Iafrate, T. R. Aucoin, and F. Rothwarf, *Bull. Am. Phys. Soc.* 21, 384 (1976).
- ⁵⁷I. Ya Nikiforov, I. I. Gegusin, and G. I. Alperovich, *Proceedings of the International Symposium on X-Ray Spectra and Electronic Structure of Matter*, Vol. II, edited by A. Faessler and G. Wiech (Fotodruck Frank Ohg., München, 1973), p. 122.
- ⁵⁸B. N. Harmon (private communication).
- ⁵⁹B. M. Klein, D. A. Papaconstantopoulos, and L. L. Boyer, *Bull. Am. Phys. Soc.* 21, 209 (1976); and unpublished.